SCIENTIFIC REP🛇RTS

OPEN

Characterization of *meta*-Cresol Purple for spectrophotometric pH measurements in saline and hypersaline media at sub-zero temperatures

Socratis Loucaides[1,2], Victoire M. C. Rèrolle[2], Stathys Papadimitriou[3], Hilary Kennedy[3], Matthew C. Mowlem[2], Andrew G. Dickson[4], Martha Gledhill[1,5] & Eric P. Achterberg[1,5]

Accurate pH measurements in polar waters and sea ice brines require pH indicator dyes characterized at near-zero and below-zero temperatures and high salinities. We present experimentally determined physical and chemical characteristics of purified meta-Cresol Purple (*m*CP) pH indicator dye suitable for pH measurements in seawater and conservative seawater-derived brines at salinities (S) between 35 and 100 and temperatures (T) between their freezing point and 298.15 K (25 °C). Within this temperature and salinity range, using purified *m*CP and a novel thermostated spectrophotometric device, the pH on the total scale (pH$_T$) can be calculated from direct measurements of the absorbance ratio R of the dye in natural samples as

$$pH_T = -\log(k_2^T e_2) + \log\left(\frac{R - e_1}{1 - R\frac{e_3}{e_2}}\right)$$

Based on the *m*CP characterization in these extended conditions, the temperature and salinity dependence of the molar absorptivity ratios and $-\log(k_2^T e_2)$ of purified *m*CP is described by the following functions: $e_1 = -0.004363 + 3.598 \times 10^{-5} T$, $e_3/e_2 = -0.016224 + 2.42851 \times 10^{-4} T + 5.05663 \times 10^{-5}(S - 35)$, and $-\log(k_2^T e_2) = -319.8369 + 0.688159\, S - 0.00018374\, S^2 + (10508.724 - 32.9599\, S + 0.059082\, S^2)$ $T^{-1} + (55.54253 - 0.101639\, S) \ln T - 0.081121 51 T$. This work takes the characterisation of *m*CP beyond the currently available ranges of $278.15\,K \leq T \leq 308.15\,K$ and $20 \leq S \leq 40$ in natural seawater, thereby allowing high quality pH$_T$ measurements in polar systems.

About half of the anthropogenic carbon dioxide (CO_2) released to the atmosphere since the industrial revolution has been absorbed by the oceans[1]. This process continues today and buffers atmospheric CO_2 levels, thereby partly alleviating global warming. The influx of CO_2 into the ocean causes acidification of surface waters and leads to a decline in the saturation states of carbonate minerals (i.e. aragonite and calcite), posing a threat to marine calcifying species[2-4]. The capacity of ocean waters to absorb CO_2 increases towards the poles because of the higher solubility of gasses at lower temperatures[5]. High freshwater inputs into polar waters, from ice and snow melt, reduce the seawater's buffering capacity, as indicated by the Revelle factor[6], leading to a decline in pH and

[1]University of Southampton, Waterfront Campus, Southampton, SO14 3ZH, UK. [2]National Oceanography Centre, European Way, Southampton, SO14 3ZH, UK. [3]Ocean Sciences, College of Natural Sciences, Bangor University, Menai Bridge, LL59 5AB, UK. [4]Marine Physical Laboratory, Scripps Institution of Oceanography, University of California, San Diego, 9500 Gilman Drive, La Jolla, CA, 92093-0244, USA. [5]GEOMAR Helmholtz Centre for Ocean Research, 24148, Kiel, Germany. Correspondence and requests for materials should be addressed to S.L. (email: s.loucaides@noc.ac.uk)

saturation states of calcite and aragonite[7, 8]. The contemporary ocean shows the lowest buffering capacity (highest Revelle factor) in polar waters[9], and it is projected that by the end of the century these regions will become under-saturated with respect to aragonite[10, 11].

Although high latitude waters contribute disproportionally to the oceanic CO_2 uptake[5, 12], the flux estimates are based on data available from periods of seasonal sea ice retreat and parts of the ocean which are ice-free[13]. Over the last few years the role of sea ice processes in CO_2 cycling has been increasingly recognised. Sea ice is a porous medium and within its pores and channels are gas pockets and residual high ionic strength liquids (brines) at thermal equilibrium with the ice[14]. The brine, enriched in seawater solutes rejected from the ice during freezing[14], is the habitat of sympagic phototrophic and heterotrophic organisms[15, 16]. It has been estimated that in first- and multi-year ice packs of the Southern Ocean, primary production results in the fixation of 36 Tg C yr^{-1} into biomass[17]. It is now accepted that the sea ice pack and land fast ice are to a measurable extent CO_2 permeable and that internal physical, chemical, and biological processes taking place during ice formation and melting may play a significant role in CO_2 cycling in high latitude oceans[18–20]. For example, gravity drainage of CO_2-rich brines during ice formation may be a significant and so far unaccounted sink of dissolved inorganic carbon (DIC) in surface waters with estimates in the order of 200–500 Tg C yr^{-1} for the (Arctic and Antarctic) polar oceans[21]. Carbonate mineral precipitation in brines during ice formation may present a potentially significant source of total alkalinity (TA) to polar surface waters following their dissolution when sea ice melts, generating an additional sink (~33–83 Tg C yr^{-1}) of atmospheric CO_2, which is equivalent to 17–42% of the air-sea CO_2 flux in open high latitude ocean waters[22]. In addition to these mechanisms (gravity drainage, $CaCO_3$ formation in sea ice), based on recent direct measurements of the CO_2 exchange between sea ice and the atmosphere as a function of ice temperature, the Antarctic ice pack, during seasonal warming, was estimated to take up the equivalent of 58% of the atmospheric CO_2 uptake of the open Southern Ocean surface waters south of 50°S[23]. The interplay between biological and physicochemical processes makes carbonate chemistry within sea ice highly complex, leading to strong gradients in pH between the ice and underlying waters with potentially significant impacts on ocean-atmosphere CO_2 fluxes[15, 18, 24–26].

Our ability to characterize the marine carbonate system in open ocean waters has undergone major advancements during the last few decades, but our understanding of CO_2 cycling in ice brine conditions remains limited due to theoretical and methodological constraints[25]. Sea ice brines exhibit a much wider range of salinity (S) and temperature (T) changes within short temporal and spatial scales than the open ocean. Specifically, brine S-T conditions in sea ice extend to the hypersaline region (S > 100) at temperatures much colder than the freezing temperatures of seawater (271.23 K at S = 35 and 0 dbar pressure)[18, 20, 27]. Such large ranges in T and S make the use of traditional *ex situ* pH and pCO_2 (partial pressure of CO_2) measurement techniques a challenge, because *in situ* temperature corrections are required post-analysis using relationships and constants that have not been validated for below- zero temperatures. The most robust method for back-calculating pH and pCO_2 to *in situ* T relies on the solution of a thermodynamic model that describes the marine CO_2 system[28]. This requires the knowledge of the first and second acidity constant of carbonic acid at *in situ* T and S. Empirical data for these constants, however, are not available to date for T < 274.15 K and S > 50 in natural seawater while non-linear extrapolation to low T and high S can potentially result in large errors in calculated pH and pCO_2 values[29].

Experimental determination of the carbonic acid acidity constants can be facilitated by measurements of all four variables (DIC, TA, pH, pCO_2) of the marine carbonate system at the S and T of interest. Although measurements of TA, DIC, and pCO_2 at sub-zero temperatures and hyper-saline conditions are possible using current methodologies and instrumentation[28], spectrophotometric pH measurements are limited to the range of conditions for which indicators have been characterised. For example, the characterization of the commonly used indicator dye meta-Cresol Purple (*m*CP) is only valid for 278.15 K ≤ T ≤ 308.15 K and 20 ≤ S ≤ 40[30, 31]. Furthermore, pH measurements at low temperatures using conventional optical apparatus (spectrophotometers, glass cells, lenses etc.) are highly problematic due to the formation of condensation along the optical path.

The purpose of this work was to facilitate pH measurements in cold and hypersaline conditions, such as those encountered in the oceanic cryosphere. To this end, we extended the characterization of the pH indicator *m*CP (in its purified form) to below-zero temperatures down to the freezing point (267.15 K) of S = 100 brines. The salinity maximum and temperature minimum were set by the S-T range in natural sea ice brines with conservative ionic composition and inter-ionic ratios relative to surface oceanic water. This development became possible by the recent electrochemical characterization of the pH of the Tris/HCl buffer system[32] and the use of a novel, custom-made microfluidic spectrophotometric system. The lens-less design of the microfluidic chip prevents condensation and is thus ideal for pH measurements at a lower range of temperatures. Our work facilitates high quality *in-situ* measurements of pH, thereby furthering our understanding of the carbonate system in polar aquatic environments.
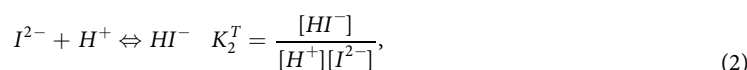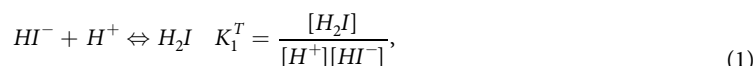
Methods

Purification of meta-Cresol Purple. The *m*CP indicator dye was obtained as a sodium salt (Acros Organics). The indicator was purified using the preparative HPLC procedure described in Liu *et al*.[31] using a Shimadzu HPLC system. In preparative mode, the system consisted of a system controller (SCL-10Avp), a preparative scale pump (LC-8A), a Rheodyne 3725i manual injector, and a diode array detector (SPD M10Avp) with a preparative flow cell. In analytical mode, the preparative pump was replaced with an analytical scale pump (LC-10ADvp) and the manual injector with an automatic injector (SIL 10AD). The HPLC column (Primesep B2) used for the purification of *m*CP was from SIELC Technologies. The Primesep B2 column uses a mixed-mode resin to separate analytes via ion-exchange and hydrophobic mechanisms. A preparative column (Part B2–220.250.0510, 22 × 250 mm, particle size 5 μm) was used for the purification procedure while a smaller

analytical column (Part B2-46-250.0510, 4.6 × 250 mm, particle size 5 μm) was used for the qualitative analysis of the purified indicator.

The mobile phase used for the purification was 70% acetonitrile (HPLC grade; Fisher Chemical) and 30% deionised water (Milli-Q, Millipore, MQW). A small amount (0.05%) of trifluoroacetic acid (TFA; ReagentPlus®; Sigma-Aldrich) was used as a mobile phase modifier. The un-purified mCP sodium salt was dissolved in the mobile phase at a concentration of 70 mM. The solution was sonicated in an ultrasonic bath for 15 min to ensure complete dissolution of the indicator. For each purification cycle, 7 mL of indicator solution was injected into the system. The pump flow rate was adjusted to 31 mL min^{-1} and the pure mCP was collected at its characteristic retention time (approximately 20 min). The pure mCP was separated from the solvent using a rotary evaporator at 40 °C under partial vacuum. Complete evaporation of the mobile phase was achieved after 2–3 h and the recovery efficiency was about 60%. The purified mCP (in acid form) was collected from the evaporation flask and its purity was tested using an analytical HPLC procedure. This was done by injecting 0.020 mL of 70 mM purified mCP (in mobile phase) through the analytical HPLC system at a flow rate of 1.5 mL min^{-1}. The mCP purity was assessed by comparing the chromatographs of the purified and unpurified material.

Characterization Procedure. Sulfonephthaleine pH indicator dyes are weak acids (H_2I) where the acidic and basic components exhibit different colours and, therefore, absorb light at distinctly different wavelengths. For mCP, H_2I is pink, HI^- is yellow and I^{-2} is purple. The relative distribution of the indicator species is pH-dependent and can be expressed in terms of chemical equilibria with corresponding dissociation constants:

$$HI^- + H^+ \Leftrightarrow H_2I \quad K_1^T = \frac{[H_2I]}{[H^+][HI^-]},$$

(1)

$$I^{2-} + H^+ \Leftrightarrow HI^- \quad K_2^T = \frac{[HI^-]}{[H^+][I^{2-}]},$$

(2)

where brackets denote concentration. At typical surface seawater pH (~8.1), mCP is present only as I^{-2} and HI^- because $pK_1^T \sim 2$ and $pK_2^T \sim 8$. At a sample pH close to the log of the indicator's second dissociation constant (pK_2^T), pH can be measured with considerable accuracy (better than 0.001) by measuring light absorption at the wavelengths of maximum absorbance of the acidic (HI^-) and basic (I^-) indicator species (434 and 578 nm, respectively).

Measurements of pH using indicator dyes require that their optical properties are carefully characterized. The characterization of mCP involves the determination under different T and S conditions of the molar absorptivity constants (ε_λ^i) of each indicator species (i) at wavelengths (λ) of 434 and 578 nm and the second dissociation constant K_2^T (equation 2). Solution pH can then be calculated from the absorbance (A_λ) ratio at 434 and 578 nm ($R = \frac{A_{578}}{A_{434}}$) using:

$$pH_T = -\log(k_2^T) + \log\left(\frac{R - e_1}{e_2 - Re_3}\right)$$

(3)

where the parameters e_1, e_2 and e_3 are the molar absorptivity ratios defined by:

$$e_1 = \frac{\varepsilon_{578}^{HI^-}}{\varepsilon_{434}^{HI^-}}; \; e_2 = \frac{\varepsilon_{578}^{I^{2-}}}{\varepsilon_{434}^{HI^-}}; \; e_3 = \frac{\varepsilon_{434}^{I^{2-}}}{\varepsilon_{434}^{HI^-}}$$

(4)

The derivation of equation 3 is described in detail in Zhang and Byrne[33].

Equation 3 can be rearranged to ref. 31:

$$pH_T = -\log(k_2^T e_2) + \log\left(\frac{R - e_1}{1 - R\frac{e_3}{e_2}}\right)$$

(5)

which simplifies the characterization procedure since e_3/e_2 is determined as a single parameter in a basic solution (pH ~12) where I^{2-} is the predominant indicator species so that:

$$\frac{e_3}{e_2} = \frac{\varepsilon_{434}^{I^{2-}}}{\varepsilon_{578}^{I^{2-}}}$$

(6)

Applying Beer-Lambert's law, and as long as $\varepsilon_{434}^{I^{2-}}$ and $\varepsilon_{578}^{I^{2-}}$ are measured in the same solutions, e_3/e_2 simply becomes the ratio between $A_{434}^{I^{2-}}$ and $A_{578}^{I^{2-}}$ eliminating the need for precise knowledge of the concentration of mCP. This, however, presents its own challenge since the absorbance of I^{2-} at 578 nm is much higher than at 434 nm making it difficult to determine both absorbances accurately from a single measurement. To overcome this, we measured the absorbances of the same solutions in two different absorption cells: 1-cm-path length for $A_{578}^{I^{2-}}$ and a 10-cm-path length for $A_{434}^{I^{2-}}$. This ensured that absorption measurements of both mCP species were within acceptable ranges and eliminated errors associated with mCP dilution preparation uncertainties. Maximum errors in the length of each absorption cell were 5 μm which translates to a maximum error of 0.045% in e_1 or e_3/e_2 and of 0.00002 in pH.

Absorption measurements for the determination of e_3/e_2 were made in *m*CP solutions with ionic composition similar to that of seawater and pH adjusted to ~12 with 1 M NaOH. To avoid precipitation of magnesium, sulphur and carbonate salts at high pH and salinities, $MgCl_2$ was replaced with $CaCl_2$ and Na_2SO_4 and $NaHCO_3$ with NaCl. The ionic strength of the solutions was adjusted accordingly to match that of seawater and brines up to S = 110. The e_3/e_2 was determined by measuring A_{434} and A_{578} in a series (n = 6–10) of *m*CP dilutions from 5–50 μM concentration.

We followed the same approach as described above for the determination of e_1, using the 1 cm cell to determine $A_{434}^{HI^-}$ and the 10 cm cell for $A_{578}^{HI^-}$. Absorbance measurements were made at *m*CP concentrations between 10 and 600 μM (n = 6–10) in NaCl solutions buffered with 0.02 M CH_3COONa with ionic strength equivalent to that of seawater and brines up to S = 110. The pH of these solutions was adjusted to 4.5 by addition of small amounts of 1 M HCl. The maximum salinity used for the determination of e_1 and e_3/e_2 (S = 110) brackets the maximum salinity at which the pH_T of the Tris/HCl buffers (S = 100) has been determined[32] (see below). The latter salinity sets the upper limit of the salinity range for the $-\log(k_2^T e_2)$ determined in this study.

The molar extinction coefficients ($\varepsilon_{434}^{I^{2-}}$, $\varepsilon_{578}^{I^{2-}}$, $\varepsilon_{434}^{HI^-}$ and $\varepsilon_{578}^{IH^-}$) were determined using the Beer-Lambert Law rearranged to $\varepsilon_\lambda^i = \frac{A_\lambda}{b \times C_{mCP}} = \frac{a}{b}$, where a is the slope of the linear regression of absorbances versus concentrations of the *m*CP dilution series and b is the length of the optical cell. Although molar extinction coefficients have been traditionally determined through repeat absorption measurements of a single *m*CP concentration (as in a single point calibration) we have opted for a multi-point regression approach to establish the linear range of our measurements and to account for intercept offsets.

The $-\log(k_2^T e_2)$ term in equation 5 was determined by the measurement of the absorbance ratio $R = \frac{A_{578}}{A_{434}}$ in Tris/HCl buffers in synthetic seawater and synthetic seawater-derived brines (S = 35–100). The buffers were prepared and their pH was characterized electrochemically on the total proton scale (pH_T) in the 267.15 K to 298.15 K temperature range with the Harned cell at the Marine Physical Laboratory, Scripps Institution of Oceanography, University of California San Diego[32]. The equimolal Tris/HCl buffer (0.08 m Tris, 0.04 m HCl) has been previously used for this purpose[31], and the salinity and temperature dependence of its pH_T in the current, extended S–T range has been determined [equimolal Tris/HCl: $pH_T = 536.08338 - 54.732367\,S + 0.8518518\,S^2 + (0.1675218 - 1.72224095 \times 10^{-2}\,S + 2.66720246 \times 10^{-4}\,S^2)\,T + (-10873.5234 + 1369.56485\,S - 21.34442\,S^2)\,T^{-1} + (-95.04342 + 9.7014355\,S - 0.1509014\,S^2)\,\ln T$ (standard error: 0.001 pH unit)][32]. However, this buffer was increasingly basic at low temperatures and high salinities (e.g., $pH_T = 8.09$ at T = 298.15 K and S = 35; $pH_T = 9.19$ at T = 269.15 K and S = 70)[32]. So, two sets of less alkaline buffers, each set with distinctly different non-equimolal Tris/HCl composition (0.06 m Tris, 0.04 m HCl; and 0.10 m Tris, 0.06 m HCl) were prepared and used for the determination of $-\log(k_2^T e_2)$ at S = 35–100. The (0.06 m Tris, 0.04 m HCl) buffers were characterized electrochemically at Scripps[32] and used for the *m*CP characterization experiments at S = 35, 45, 50, 60, 70, 85, and 100. Their pH_T was calculated from the reported best-fit function, $pH_T = 144.4361 - 1.0809685\,S + 0.006023772\,S^2 + (0.0618411 - 0.000817397\,S + 4.27187 \times 10^{-6}\,S^2)\,T + (-27.233738 + 0.2329236\,S - 0.001281138\,S^2)\,\ln T$, with a standard error of 0.002 pH unit[32]. The (0.10 m Tris, 0.06 m HCl) buffers were used for additional *m*CP characterization experiments at S = 35 and 45. The pH_T of the (0.10 m Tris, 0.06 m HCl) buffers was not characterized electrochemically (except for the S = 45 buffer at 273.15 K, see below) but instead computed from the equimolal pH_T (as calculated from the best-fit equation cited above) via the Henderson–Hasselbalch equation[32, 34]. This computation gives $pH_T = 8.785$ at 273.15 K for the S = 45 (0.10 m Tris, 0.06 m HCl) buffer, which agrees well with the value determined electrochemically ($pH_T = 8.783$) as described in Papadimitriou *et al.*[32]. This approach is also supported from the excellent agreement between thus computed and electrochemically determined pH_T values for the (0.06 m Tris, 0.04 m HCl) buffers[32].

Spectrophotometric measurements.

The experimental set-up used for the determination of molar absorptivity constants (ε_λ^i) is illustrated in Fig. 1. The microfluidic flow cells used for the characterization were manufactured in tinted poly (methyl methacrylate) (PMMA). The fabrication procedure is described in detail in Ogilvie *et al.*[35] and Floquet *et al.*[36]. Two absorption cells (1 cm and 10 cm) with cross sections of 700 μm × 700 μm were micro-milled into a single PMMA chip. A tungsten halogen light source (Ocean Optics HL-2000) was used for the absorption measurements in conjunction with a 434 nm LED used to boost light intensity at the lower end of the spectrum. A linear array photodiode spectrophotometer (USB4000, Ocean Optics, UK) was used as a detector. Both the light source and detector were connected to the microfluidic flow cell with 600 μm diameter optical fibres (Thorlabs, USA). The flow cell was submerged in a water bath (Grant TX150) filled with 15% ethylene glycol solution. The temperature was kept constant (±0.02 °C) and was monitored continuously using a precision thermometer (ASL F250 MKII). The lens-less design of the PMMA microfluidic flow cell allowed for uncompromised optical measurements of pH (no condensation issues) and superior thermostatic control at near-freezing temperatures.

For the determination of the molar absorptivity constants (ε_λ^i), experimental solutions were volumetrically premixed with *m*CP indicator using calibrated pipettes in 20 mL glass vials with silicone/PTFE septum tops. The vials were kept on a rack which was submerged in the water bath. Solutions were siphoned from the vials through a 0.7 mm i.d. PTFE capillary tube into the flow cell using a 1 mL disposable syringe connected to the outlet of the flow cell. The flow cell was flushed with 2 mL of the experimental solution between measurements. The absorption spectrum was recorded in replicate (n = 5) using LabVIEW® software. Reference measurements were performed in experimental solutions without added indicator.

For the determination of $-\log k_2^T e_2$, the $R = \frac{A_{578}}{A_{434}}$ was determined inTris/HCl buffers using the microfluidic pH sensor as described in Rérolle *et al.*[37] but with the same spectrophotometer and light source described above. For each measurement, 4 μL of the 4 mM *m*CP solution was mixed with 900 μL Tris/HCl buffer. The impact of the
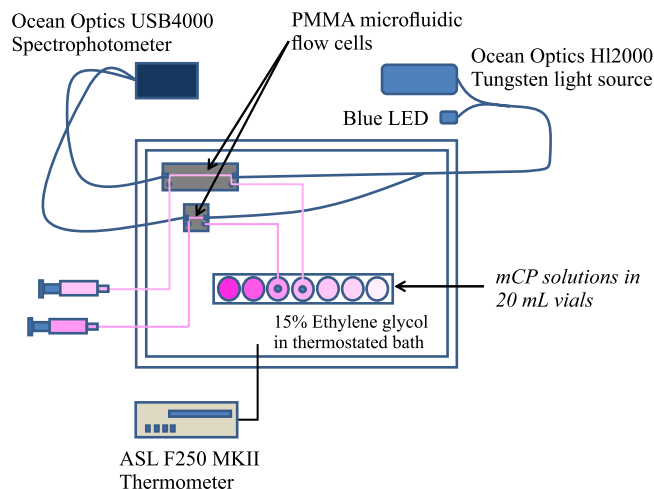
Figure 1. Experimental setup used for the determination of the molar absorptivity ratios e$_1$ and e$_3$/e$_2$. The microfluidic flow cells and vials with *m*CP solutions are submerged in a 15% ethylene glycol thermostated bath. The light is transmitted from the light source to the flow cells and to the spectrophotometer through 600 µm diameter optical fibres (Thorlabs, USA).
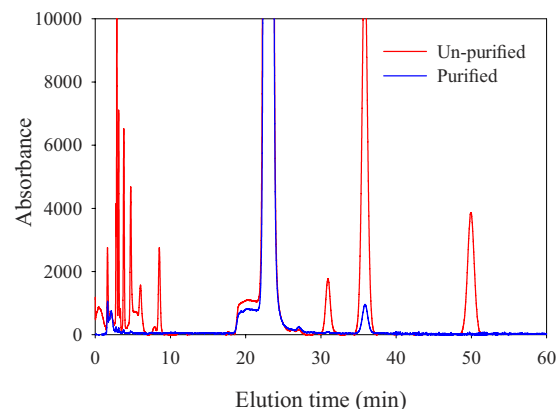

Figure 2. HPLC chromatogram of un-purified (red line) and purified (blue line) *m*CP. Note that traces of a component eluted at approximately 36 minutes are still present in the purified indicator.

*m*CP addition on the buffer pH was estimated by measuring pH over a wide range of *m*CP to buffer mixing ratios (1:25 to 1:80) and using this data to regress back to a theoretical pH where *m*CP concentration was zero. This range of mixing ratios was obtained from the dispersion of *m*CP in Tris/HCl buffer within the microfluidic channels[37]. The measurements for the determination of $-\log k_2^T e_2$ were conducted at 273.15 K and below-zero temperatures to near the freezing point of the synthetic buffer solutions, as well as at 298.15 K, 283.15 K, and 278.15 K for overlap and direct comparison with the existing data set for purified *m*CP in Liu *et al*.[31] An estimate of the freezing point of the synthetic buffer solutions was computed from the empirical absolute salinity-temperature relationship of thermally equilibrated sea ice brines[38], $S_A = 1000 \, [1-(54.11/t)]^{-1}$ where t is the temperature in °C.

Results and Discussion

Purification of meta-Cresol Purple.
Impurities in indicator dyes result in significant uncertainties in measured pH values[31, 39]. Analyses have shown that commercially available *m*CP indicators contain different types and quantities of light absorbing impurities, which could lead to pH offsets as large as 0.01 pH units. Therefore, characterizations of un-purified *m*CP are batch-specific and only valid for pH measurements using the same indicator batch. Measurements generated using uncharacterised un-purified *m*CP can be post-corrected as long as stocks of the un-purified indicator used are archived[31]. The HPLC purification procedure developed by Liu *et al*.[31] was closely replicated here, yielding approximately 150 mg of purified *m*CP from each injection. Analysis of the un-purified *m*CP indicator following the analytical HPLC protocol of Liu *et al*.[31] revealed a near identical chromatogram with the exception of an additional peak eluted at about 50 min (Fig. 2). Analysis of the purified material using the same protocol showed complete removal of impurities, with an exception of trace amounts (<8%) of a component eluted at 36 min. Similar residual profiles have been found after purification but have been reported to have practically no effect (<0.001 pH unit) on pH measurements in buffer solutions[40].
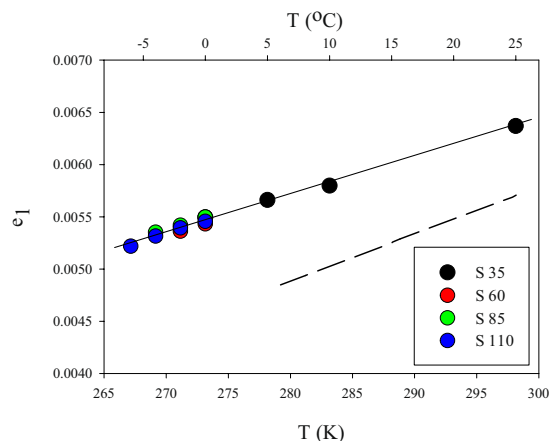
Figure 3. Values of e_1 as a function of temperature, obtained in NaCl solutions buffered with CH_3COONa (pH ~4.5) with ionic strengths equivalent to salinities of 35, 60, 85 and 110. The dashed line represents the e_1 relationship determined by Liu *et al.*[31].

Molar absorptivity ratios as a function of temperature and salinity.

e_1 as a function of temperature. The temperature dependence of e_1 for $267.15\,K \leq T \leq 298.15\,K$ and $35 < S < 110$ is relatively small (Fig. 3) and is described by the best-fit equation:

$$e_1 = -0.004363 + 3.598 \times 10^{-5}\,T, \qquad (7)$$

Although at pH 4.5 the dominant indicator species is HI^-, small absorbance contributions at 434 and 578 nm from I^{2-} and H_2I have not been accounted for in our experiments. This may explain why, between 278.15 K and 308.15 K, the best-fit equation (7) above produces e_1 values between 20% and 10%, respectively, higher than those of Liu *et al.*[31] (Fig. 3), who found that removing this bias reduced their e_1 values by a similar magnitude (14–18%). The I^{2-} and H_2I absorbance contributions are, nonetheless, relatively small, and their effect on pH measurement is minor (<0.0008 pH units) at high R values (>0.7) and slightly larger (up to 0.0034 pH units) at low R values (0.1–0.7)[31]. Refinement of e_1 to account for the contributions of I^{2-} and H_2I is possible using an iterative procedure and experimental determinations of $\varepsilon_{434}^{H_2I}$, $\varepsilon_{578}^{H_2I}$, and the K_1 of mCP[31]. This, however, requires careful and laborious experiments offering only minor gain in pH measurement performance especially at pH > 7.5. The potential error in the e_1 computation from equation (7) above due to the unaccounted absorbance contributions of I^{2-} and H_2I is not necessarily propagated to the final pH determination (equation 5) but is likely "calibrated out" during the determination of $-\log(k_2^T e_2)$ as described subsequently.

Changes in salinity have no significant effect on e_1 between $S = 35$ and $S = 110$ (Fig. 3), consistent with the findings of Liu *et al.*[31]. Generally, e_1 has a minor influence on the calculation of pH at high pH values (>8). At pH 8, it is possible to disregard the temperature dependence of e_1 and use an average value with no significant impact on pH (<0.001 pH units) or disregard it altogether ($e_1 = 0$) with only a minor effect on pH (0.002 pH units).

e_3/e_2 as a function of temperature and salinity. The e_3/e_2 term in equation 5 is influenced by both the ionic strength and ionic composition[31] and, for this reason, was determined in an electrolyte solution with near-seawater composition and carefully adjusted ionic strength. The pH was adjusted to ~12 with NaOH so that only the basic (I^{2-}) form of mCP was present and interferences from HI^- and H_2I were negligible. The temperature and salinity dependence of e_3/e_2 (Fig. 4) for $267.15\,K < T < 298.15\,K$ and $35 < S < 110$ can be described by:

$$e_3/e_2 = -0.016224 + 2.42851 \times 10^{-4}\,T + 5.05663 \times 10^{-5}\,(S - 35) \qquad (8)$$

The relationship provides e_3/e_2 values that are in agreement with those reported by Liu *et al.*[31]; at $S = 35$ and $T = 298.15\,K$, the difference between the values obtained from equation 8 and from the relationship in Liu *et al.*[31] is 0.0006, which corresponds to a pH discrepancy of less than 0.001 for pH values lower than 8.3. This discrepancy becomes even smaller at lower temperatures. At higher salinities, however, the deviation between the e_3/e_2 predicted by the equation of Liu *et al.*[31] and its value computed from equation 8 above increases to about 0.005, equivalent to ΔpH = 0.010, at $S = 100$. The expression for e_3/e_2 by Liu *et al.*[31] was optimized for S between 20 and 40, which consequently results in an enhanced discrepancy with our findings at higher salinities. Extrapolation of the Liu *et al.*[31] e_3/e_2 relationship to salinities higher than $S = 40$ is therefore not advisable. Equation 8 was not experimentally validated at $S < 35$; nevertheless, it agrees well with that of Liu *et al.*[31] at $S = 20$ (the low end of their experimental range), with a maximum discrepancy at 273.15 K of 0.0006 (ΔpH = 0.002).

The pH values obtained using equation 5 are sensitive to variations in e_3/e_2 and, therefore, experimental determination requires due care. The multi-point determination of the molar absorptivities of I^{2-} ($\varepsilon_{434}^{I^{2-}}$, $\varepsilon_{578}^{I^{2-}}$) showed that the intercept of the regression of absorbance *versus* concentration cannot always be assumed as zero. We have observed small but significant intercept offsets in the e_3/e_2 determination experiments that, if ignored (e.g., through single point determination), could result in pH errors of ca. 0.001 pH unit. It is not clear what the source
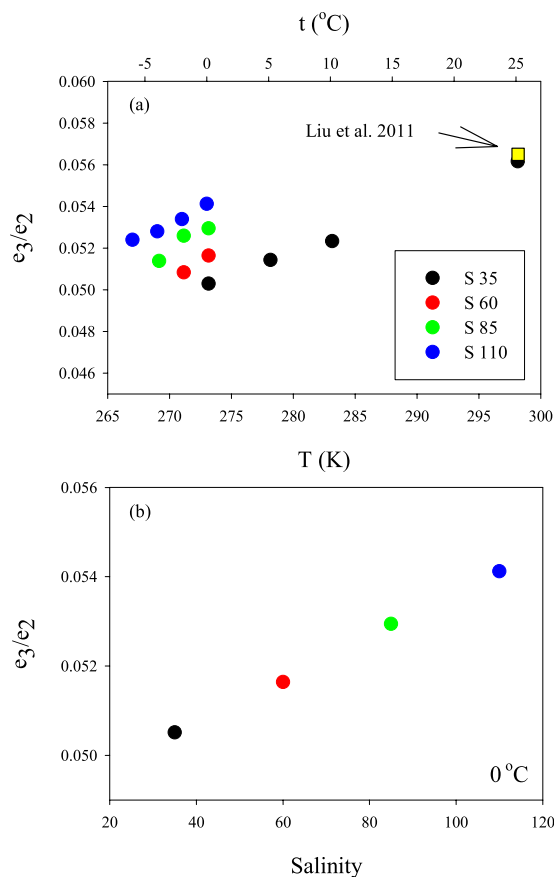
Figure 4. Values of e_3/e_2 (**a**) as a function of temperature, and (**b**) salinity at 0 °C. The measurements were obtained at pH 12 in solutions with near-seawater composition and ionic strength equivalent to salinities 35, 60, 85, and 110. The yellow square in panel (a) represents the e_3/e_2 value reported by Liu et al.[30] for S = 35 and T = 298.15 K.

of the non-zero intercept is in our experiments, but it may be related to light instabilities of the optical system or other random errors. Benchtop dual-beam spectrophotometers are inherently more stable, allowing for higher quality optical measurements. It is therefore possible that using such instruments eliminates the need for the multi-point determination approach used in this work. This, however, remains to be tested, and it is recommended that, when portable spectrophotometers are used (as in this work), a multi-point determination approach is used.

Determination of $-\log(k_2^T e_2)$ as a function of temperature and salinity.

The temperature and salinity dependence of $-\log(k_2^T e_2)$ of purified mCP was determined by measurements of the absorbance ratio ($R = A_{578}/A_{434}$) in the Tris/HCl buffers prepared in a range of salinities (S = 35, 45, 50, 60, 70, 85, and 100) at temperatures ranging from their freezing point to 298.15 K. The temperature and salinity dependence of $-\log(k_2^T e_2)$ in these conditions can be described by:

$$-\log(k_2^T e_2) = a + \frac{b}{T} + c \ln T + dT,$$

(9)

The factors in the above equation were determined from our measurements using the regression routine in Excel, with $a = -319.8369 + 0.688159\ S - 0.00018374\ S^2$, $b = 10508.724 - 32.9599\ S + 0.059082\ S^2$, $c = 55.54253 - 0.101639 S$, $d = -0.08112151$ ($r^2 = 0.9986$, $p < 0.00001$, $n = 47$, standard error of fit: $\sigma_{fit} = 0.007$). Based on this equation, $-\log(k_2^T e_2) = 8.0171$ at 0 °C and S = 35, while $-\log(k_2^T e_2) = 8.2475$ at −6 °C and S = 100. The relatively strong temperature dependence of $-\log(k_2^T e_2)$ (Fig. 5) highlights the importance of accurate temperature control (±0.05 °C) during pH measurements. Accurate knowledge of salinity is less important (±1 psu), especially within ranges associated with open ocean waters (30 < S < 40). Under these conditions, salinity variations of the order of 1 psu have only a minor effect on $-\log(k_2^T e_2)$ and pH (0.001–0.002 unit) within the uncertainty of the $-\log(k_2^T e_2)$ value, based on the standard error of the best-fit S-T function above. At higher salinities (S > 50), more accurate salinity measurements (0.1 psu) are desirable to maintain the same magnitude of $-\log(k_2^T e_2)$ and pH uncertainty (in the order of 0.001 pH unit at S = 90).
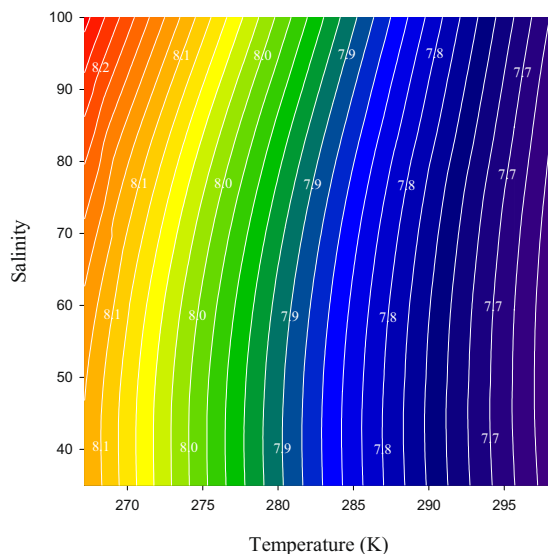
Figure 5. Temperature and salinity dependence of $-\log(k_2^T e_2)$ (values on contour lines) as determined in this study from the absorbance ratio ($R = A_{578}/A_{434}$) measurements in electrochemically characterized Tris/HCl buffers in synthetic seawater and brines (S = 35, 45, 50, 60, 70, 85, and 100) between their freezing point and 298.15 K.
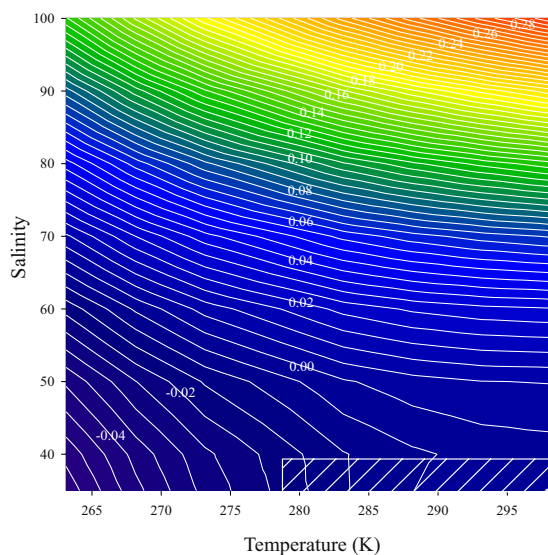

Figure 6. Differences in $-\log(k_2^T e_2)$ calculated with the Liu *et al.* (2011) and current parameterizations (equation 8). The hatched rectangle represents a portion of the experimental range of Liu *et al.*[31].

Liu *et al.*[31] determined the $-\log(k_2^T e_2)$ of purified *m*CP for $278.15 \leq T \leq 308.15$ and S = 20–40. Our $-\log(k_2^T e_2)$ S-T parameterization (equation 9) and that in Liu *et al.*[31] yield values within 0.001 at S = 35 and T = 298.15 ± 5 K and within 0.010 down to T = 283.15 K. Higher discrepancies between the two relationships at low temperatures (Fig. 6) may reflect differences between the instruments used for the $-\log(k_2^T e_2)$ determination. The pH measuring system used for this work had no parts of the optical path exposed to air, thus eliminating the possibility of condensation at low temperatures. The condensation is more difficult to control with bench-top spectrophotometers as that used by Liu *et al.*[31], although dry N_2 gas was used to eliminate condensation on the optical windows at 5 °C. From this comparison, it is clear that the relationship for $-\log(k_2^T e_2)$ by Liu *et al.*[31] should not be extrapolated for pH measurements outside its range (S = 20–40, T = 278.15–303.15 K) as this can lead to large errors in pH (0.02–0.30) (Fig. 6). The relationship (equation 8) proposed here should also not be used outside its calibration range (S = 35–100, T = 267.15–298.15 K).
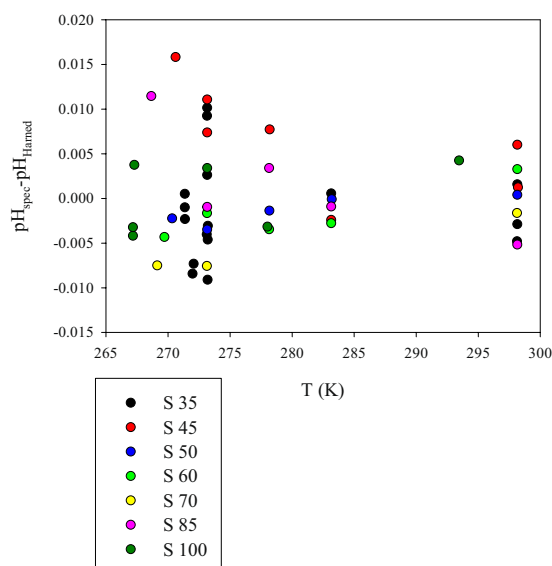
Figure 7. Differences between spectrophotometrically (equations 4, 6, 7 and 8) and electrochemically (Harned) determined pH_T in Tris/HCl buffer solutions in synthetic seawater and brines with conservative (seawater-derived) major ionic composition.

Determination of pH using purified *m*CP at temperatures between 298.15 K and the freezing point of seawater and sea-ice brines up to salinity 100. Equations 5, 7, 8, and 9 can be used to determine pH on the total proton scale by measurement of the absorption ratio R of purified *m*CP in seawater and seawater brines, with conservative major ionic composition, with S between 30 and 100 and T between freezing point and 298.15 K. The residuals ($pH_{spec}-pH_{Harned}$) of pH measurements in Tris/HCl buffers using purified *m*CP and application of eq. 4, 6, 7 and 8 indicate a relatively wide spread (Fig. 7) with an average absolute residual of 0.004 and maximum absolute residual of 0.016. As the analytical precision (1 standard deviation of n = 5–10 repeat measurements of the same buffer) is significantly smaller (0.001–0.004), at least part of the observed magnitude of buffer residuals could be attributed to error propagation from the parameters involved in pH determination (e.g., $-\log(k_2^T e_2)$, $\sigma_{fit} = 0.007$) and random error related to buffer preparation, bottling, and handling. Residuals are up to 3 times larger close to the freezing point than at 298.15 K possibly due to the physical/optical heterogeneity of water during the early stages of ice-crystal formation. Therefore, the proposed pH measurement protocol offers good precision (0.001–0.004) and an overall uncertainty in the order of the maximum residual values observed here (0.010–0.020 pH unit), especially at below-zero temperatures near the freezing point of concentrated brines. In comparison, extrapolation of the temperature and salinity dependence of the *m*CP characterization by Liu *et al.*[31] to values outside their empirical range can lead to pH errors at S = 100 in the order of 0.3 pH unit.

Summary and Conclusion

We have purified *m*CP and characterized it spectrophotometrically in synthetic solutions with conservative seawater major ionic composition and salinity between 35 and 100 at temperatures ranging from the freezing point of such solutions to 298.15 K. This was made possible by the use of suitable and well characterised Tris/HCl buffers and a novel custom-made optical cell that was fully submerged in a water bath eliminating the possibility of condensation build-up in the optical path. This setup allowed for accurate optical measurements at temperatures down to 267.15 K. Both the experimental set-up and the S-T functions of this work will allow traceable, precise, and reliable spectrophotometric pH measurements in internal sea ice brines and other high latitude and deep waters where temperatures are often just above freezing. The current characterization of purified mCP offers major improvement of pH measurement (0.010–0.020 pH unit uncertainty) in high salinities (up to S = 100) and near-zero and below-zero temperatures to the freezing point over that obtained from the extrapolation of the previous characterization[30] (0.3 pH unit uncertainty) to these S-T conditions. The important tools developed in this work provide a step forward towards the understanding of the carbonate system in the cryosphere and cold waters in general. In combination with attainable measurements of the remainder three measurable parameters of the carbonate system (DIC, TA, pCO$_2$), the reliable pH measurements made possible in the extended salinity and temperature ranges of this investigation will facilitate the determination of several unknowns in the parameterization of the carbonate system in these S –T conditions, including the acidity constants of carbonic acid and, following this, important geochemical indicators, such the saturation state of seawater and brines with respect to carbonate minerals in high latitude marine systems.

References

1. Feely, R. A. *et al*. Impact of Anthropogenic CO2 on the CaCO3 System in the Oceans. *Science* **305**, 362–366, doi:10.1126/science.1097329 (2004).
2. Aze, T. *et al*. An Updated Synthesis of the Impacts of Ocean Acidification on Marine Biodiversity (CBD Technical Series; 75). (Secretariat of the Convention on Biological Diversity, 2014).
3. Doney, S. C., Fabry, V. J., Feely, R. A. & Kleypas, J. A. Ocean Acidification: The Other CO2 Problem. *Annual Review of Marine Science* **1**, 169–192, doi:10.1146/annurev.marine.010908.163834 (2009).
4. Kroeker, K. J., Kordas, R. L., Crim, R. N. & Singh, G. G. Meta-analysis reveals negative yet variable effects of ocean acidification on marine organisms. *Ecol. Lett.* **13**, 1419–1434, doi:10.1111/j.1461-0248.2010.01518.x (2010).
5. Takahashi, T. *et al*. Global sea-air CO2 flux based on climatological surface ocean pCO2, and seasonal biological and temperature effects. *Deep Sea Res. II: Top. Stud. Oceanogr* **49**, 1601–1622 (2002).
6. Revelle, R. & Suess, H. E. Carbon Dioxide Exchange Between Atmosphere and Ocean and the Question of an Increase of Atmospheric CO2 during the Past Decades. *Tellus* **9**, 18–27, doi:10.1111/j.2153-3490.1957.tb01849.x (1957).
7. Chierici, M. *et al*. Impact of biogeochemical processes and environmental factors on the calcium carbonate saturation state in the Circumpolar Flaw Lead in the Amundsen Gulf, Arctic Ocean. *J. Geophys. Res.* **116**, C00G09, doi:10.1029/2011jc007184 (2011).
8. Yamamoto, A., Kawamiya, M., Ishida, A., Yamanaka, Y. & Watanabe, S. Impact of rapid sea-ice reduction in the Arctic Ocean on the rate of ocean acidification. *Biogeosciences* **9**, 2365–2375, doi:10.5194/bg-9-2365-2012 (2012).
9. Sabine, C. L. *et al*. The Oceanic Sink for Anthropogenic CO2. *Science* **305**, 367–371, doi:10.1126/science.1097403 (2004).
10. Caldeira, K. & Wickett, M. E. Anthropogenic carbon and ocean pH: The coming centuries may see more ocean acidification than the past 300 million years. *Nature* **425**, 365 (2003).
11. Orr, J. C. *et al*. Anthropogenic ocean acidification over the twenty-first century and its impact on calcifying organisms. *Nature* **437**, 681–686 (2005).
12. Bates, N. R. & Mathis, J. T. The Arctic Ocean marine carbon cycle: evaluation of air-sea CO2 exchanges, ocean acidification impacts and potential feedbacks. *Biogeosciences* **6**, 2433–2459 (2009).
13. Miller, L. A. *et al*. Changes in the marine carbonate system of the western Arctic: patterns in a rescued data set. *Polar Res.* **33**, 1–15, doi:10.3402/polar.v33.20577 (2014).
14. Cox, G. F. N. & Weeks, W. F. Equations for determining the gas and brine volumes in sea-ice samples. *Journal of Glaciology* **29**, 306–316 (1983).
15. Papadimitriou, S. *et al*. Biogeochemical composition of natural sea ice brines from the Weddell Sea during early austral summer. *Limnol. Oceanogr.* **52**, 1809–1823, doi:10.4319/lo.2007.52.5.1809 (2007).
16. Thomas, D. N. & Dieckmann, G. S. Antarctic Sea Ice–a Habitat for Extremophiles. *Science* **295**, 641–644, doi:10.1126/science.1063391 (2002).
17. Arrigo, K. R., Worthen, D. L., Lizotte, M. P., Dixon, P. & Dieckmann, G. Primary Production in Antarctic Sea Ice. *Science* **276**, 394–397, doi:10.1126/science.276.5311.394 (1997).
18. Miller, L. A., Carnat, G., Else, B. G. T., Sutherland, N. & Papakyriakou, T. N. Carbonate system evolution at the Arctic Ocean surface during autumn freeze-up. *Journal of Geophysical Research: Oceans* **116**, C00G04, doi:10.1029/2011JC007143 (2011).
19. Miller, L. A. *et al*. Carbon dynamics in sea ice: A winter flux time series. *Journal of Geophysical Research: Oceans* **116**, n/a-n/a, doi:10.1029/2009JC006058 (2011).
20. Papadimitriou, S. *et al*. The effect of biological activity, CaCO3 mineral dynamics, and CO2 degassing in the inorganic carbon cycle in sea ice in late winter-early spring in the Weddell Sea, Antarctica. *Journal of Geophysical Research: Oceans* **117**, n/a-n/a, doi:10.1029/2012JC008058 (2012).
21. Rysgaard, S., Glud, R. N., Sejr, M. K., Bendtsen, J. & Christensen, P. B. Inorganic carbon transport during sea ice growth and decay: A carbon pump in polar seas. *Journal of Geophysical Research: Oceans* **112**, n/a-n/a, doi:10.1029/2006jc003572 (2007).
22. Rysgaard, S. *et al*. Sea ice contribution to the air–sea CO2 exchange in the Arctic and Southern Oceans. *Tellus B* **63**, 823–830, doi:10.1111/j.1600-0889.2011.00571.x (2011).
23. Delille, B. *et al*. Southern Ocean CO2 sink: The contribution of the sea ice. *Journal of Geophysical Research: Oceans* **119**, 6340–6355, doi:10.1002/2014JC009941 (2014).
24. Gleitz, M., v.d. Loeff, M. R., Thomas, D. N., Dieckmann, G. S. & Millero, F. J. Comparison of summer and winter inorganic carbon, oxygen and nutrient concentrations in Antarctic sea ice brine. *Mar. Chem.* **51**, 81–91, doi:10.1016/0304-4203(95)00053-T (1995).
25. Hare, A. A. *et al*. pH Evolution in Sea Ice Grown at an Outdoor Experimental Facility. *Mar. Chem.* doi:10.1016/j.marchem.2013.04.007 (2013).
26. Papadimitriou, S., Kennedy, H., Kattner, G., Dieckmann, G. S. & Thomas, D. N. Experimental evidence for carbonate precipitation and CO2 degassing during sea ice formation. *Geochim. Cosmochim. Acta* **68**, 1749–1761, doi:10.1016/j.gca.2003.07.004 (2004).
27. Fofonoff, N. P. & Millard, R. C. Algorithms for computation of fundamental properties of seawater. (UNESCO, 1983).
28. Dickson, A. G., Sabine, C. L. & Christian, J. R. *Guide to Best Practices for Ocean CO₂ Measurements*. Vol. 3 (PICES Special Publication, 2007).
29. Brown, K. A., Miller, L. A., Davelaar, M., Francois, R. & Tortell, P. D. Over-determination of the carbonate system in natural sea-ice brine and assessment of carbonic acid dissociation constants under low temperature, high salinity conditions. *Mar. Chem.* **165**, 36–45, doi:10.1016/j.marchem.2014.07.005 (2014).
30. Clayton, T. D. & Byrne, R. H. Spectrophotometric seawater pH measurements: total hydrogen ion concentration scale calibration of m-cresol purple and at-sea results. *Deep Sea Res. I: Oceanogr. Res. Pap* **40**, 2115–2129 (1993).
31. Liu, X., Patsavas, M. C. & Byrne, R. H. Purification and Characterization of meta-Cresol Purple for Spectrophotometric Seawater pH Measurements. *Environ. Sci. Technol.* **45**, 4862–4868, doi:10.1021/es200665d (2011).
32. Papadimitriou, S. *et al*. The measurement of pH in saline and hypersaline media at sub-zero temperatures: Characterization of Tris buffers. *Mar. Chem.* **184**, 11–20, doi:10.1016/j.marchem.2016.06.002 (2016).
33. Zhang, H. N. & Byrne, R. H. Spectrophotometric pH measurements of surface seawater at *in-situ* conditions: Absorbance and protonation behavior of thymol blue. *Mar. Chem.* **52**, 17–25, doi:10.1016/0304-4203(95)00076-3 (1996).
34. Pratt, K. W. Measurement of pHT values of Tris buffers in artificial seawater at varying mole ratios of Tris:Tris·HCl. *Mar. Chem.* **162**, 89–95, doi:10.1016/j.marchem.2014.03.003 (2014).
35. Ogilvie, I. R. G. *et al*. Reduction of surface roughness for optical quality microfluidic devices in PMMA and COC. *Journal of Micromechanics and Microengineering* **20**, 065016 (2010).
36. Floquet, C. F. A. *et al*. Nanomolar detection with high sensitivity microfluidic absorption cells manufactured in tinted PMMA for chemical analysis. *Talanta* **84**, 235–239, doi:10.1016/j.talanta.2010.12.026 (2011).
37. Rérolle, V. M. C. *et al*. Development of a colorimetric microfluidic pH sensor for autonomous seawater measurements. *Anal. Chim. Acta* **786**, 124–131, doi:10.1016/j.aca.2013.05.008 (2013).
38. Assur, A. Composition of sea ice and its tensile strength in Arctic sea ice. 106–138 (National Academy of Sciences, 1958).
39. Yao, W. S., Liu, X. W. & Byrne, R. H. Impurities in indicators used for spectrophotometric seawater pH measurements: Assessment and remedies. *Mar. Chem.* **107**, 167–172, doi:10.1016/j.marchem.2007.06.012 (2007).
40. Patsavas, M. C., Byrne, R. H. & Liu, X. W. Purification of meta-cresol purple and cresol red by flash chromatography: Procedures for ensuring accurate spectrophotometric seawater pH measurements. *Mar. Chem.* **150**, 19–24, doi:10.1016/j.marchem.2013.01.004 (2013).

Author Contributions

S.L. conducted the experiments, analysed the data, made the figures and wrote the manuscript. V.R. developed and built the spectrophotometric pH apparatus and measured the pH of the buffers. S.P. prepared and characterised the buffers and contributed to the analysis of the data. H.K. as the project's principal investigator managed the project. M.M. oversaw and contributed to the development of the relevant technology. A.D. lead the production and characterisation of the buffers. M.G. set up and optimised the indicator purification procedure. E.A. contributed to the data analysis and interpretation. All authors reviewed the manuscript.

Additional Information

Competing Interests: The authors declare that they have no competing interests.

Publisher's note: Springer Nature remains neutral with regard to jurisdictional claims in published maps and institutional affiliations.